# Electron scattering on two-neutron halo nuclei with full inclusion of final state interactions

S. N. Ershov,* B. V. Danilin,† and J. S. Vaagen
*SENTEF Department of Physics and Technology, University of Bergen, Norway*
(Received 14 April 2005; published 28 October 2005)

A theory for electron scattering from Borromean two-neutron halo nuclei with full inclusion of final state interactions is developed. The halo nucleus is described as a three-body system (core + $n$ + $n$). Nuclear wave functions for bound state and low-lying three-body continuum excitations are calculated by the method of hyperspherical harmonics. The model is applied to explore electron scattering on $^6$He leading to nuclear excitations near the three-body breakup threshold.

DOI: 10.1103/PhysRevC.72.044606 PACS number(s): 21.45.+v, 21.60.Gx, 25.30.Fj, 25.60.−t

## I. INTRODUCTION

One of the most interesting questions in the physics of radioactive beams is that of the structure of halo nuclei at the limits of nuclear existence. In Borromean two-neutron halo nuclei, such as $^6$He and $^{11}$Li, the nature of the three-body continuum is most intriguing. The concentration of transition strength, experimentally observed in these nuclei at low excitation energies, may contain three-body resonances or new kinds of collective motion, such as a soft dipole mode corresponding to oscillations of the core against the halo neutrons. The continuum is usually explored via responses induced by transitions from the ground state to the continuum. A possible way to study the continuum properties is to explore nuclear reactions under conditions where one-step transitions dominate. This is, however, still a rather comprehensive task, because of the intertwining of the ground state and continuum structures, influenced by reaction mechanisms.

Because of the unstable nature of halo nuclei, their experimental studies have so far been performed with reactions involving collisions in inverse kinematics. The theoretical analysis of such reactions involves strong nucleon-nucleon interactions. The strength and complicated character of strong interactions bring ambiguities in disentangling the reaction mechanism and the nuclear structure. In spite of a considerable amount of nuclear structure information on halo nuclei extracted from collisions with other nuclei, cleaner ways for studying aspects of their structures are greatly needed.

Electron scattering is one of the most powerful and proved methods for nuclear structure investigation. The electromagnetic interaction of an electron with nuclear charges and currents is well known and weak. Thus, in principle, the reaction mechanism can be disentangled from the nuclear structure effects. Since the charge of light halo nuclei resides in only a few protons, multiple scattering effects for ultrarelativistic electrons used in nuclear structure studies can safely be neglected, and the interactions can be well described by one-photon exchange terms. At the present moment there is no ready installation for performing electron scattering experiments on unstable nuclei. Electron-nucleus collider experiments are planned, however, for future installations at RIKEN and GSI. The first measurements will be done for the processes with the largest cross sections, elastic and inclusive inelastic electron scattering.

Two articles concerning the theoretical calculations of electron scattering from two-neutron halo nuclei have already been published [1,2]. The model developed there is based on the assumption that the total energy and momentum transfer is absorbed by one of the nuclear constituents (participant) only, which is knocked out from the halo system, having the other two mutually interacting fragments as a pair of spectators. The final state interaction between the participant and the spectators is neglected in the model. This participant-spectator picture is reasonable for kinematic regions where quasi-elastic processes dominate. But the characteristic features of the Borromean halo structure are most strongly revealed at other kinematical conditions: at low-energy nuclear excitations just above the three-body breakup threshold. Here the fragments have low relative kinetic energies and correspondingly low relative velocities. They have enough time for mutual interactions, and the participant-spectator model is not justified anymore: all fragments are active in the reaction process. The correct physical description demands an inclusion of final state interactions (FSIs) in full scale, i.e. between all three constituents.

Our aim in this article is to develop a model for description of electron scattering processes leading to low-energy excitations of Borromean two-neutron halo nuclei, taking final state interactions between the fragments fully into account. The key elements include a consistent treatment of three-body features of the halo structure not only in bound states but also in continuum. The model is suitable for describing processes of the breakup into three fragments at small momentum and energy transfers and is applied to the case of electron scattering on the $^6$He nucleus, which serves as a test-bench example for two-neutron halo systems. Note that a similar model for electron scattering on three nucleon nuclei ($^3$H, $^3$He) with full inclusion of FSIs in momentum space was developed in Refs. [3,4] some years ago. These works strongly underline the importance of full FSI inclusion for breakup processes.

*Permanent address: Joint Institute for Nuclear Research, RU-141980 Dubna, Russia. Electronic address: ershov@thsunl.jinr.ru
†Permanent address: Russian Research Center "The Kurchatov Institute," RU-123182 Moscow, Russia.

 

## II. ELECTRON SCATTERING FORMALISM.

### A. General consideration

We consider a reaction process in which an electron with energy $\varepsilon_i$ and momentum $\hbar\mathbf{k}_i$ hits a nucleus with mass $\mathcal{M}_i$ and scatters with final energy $\varepsilon_f$ and momentum $\hbar\mathbf{k}_f$. The initial $k_i = (\varepsilon_i/\hbar c, \mathbf{k}_i)$, final $k_f = (\varepsilon_f/\hbar c, \mathbf{k}_f)$ and transferred $q = k_i - k_f = (\omega/c, \mathbf{q})$ four-dimensional wave vectors characterize the reaction. A derivation of electron scattering cross sections can be found in many reviews and monographs (see, for example, Refs. [5–7]). To justify the definitions of our nuclear matrix elements and approximations involved, we briefly give some intermediate steps on the way to final formulas.

Because of the weakness of the electromagnetic interaction, the one-photon exchange approximation between the electron and the nuclear system is very accurate for ultrarelativistic electron scattering from light nuclei. Within this approximation the electron cross section averaged over the initial and summed over the final spin projections can be written as follows [5,8]:

$$d\sigma = d\varepsilon_f d\Omega_f \sigma_M \sum_{\lambda\lambda'} l_{\lambda\lambda'}(-1)^{\lambda+\lambda'} N_{\lambda\lambda'}, \tag{1}$$

where summation is over photon helicities $\lambda = 0, \pm 1$ and $\sigma_M$ is the Mott cross section that describes electron scattering on a pointlike nucleus. In Eq. (1), $l_{\lambda\lambda'}$ is the well-known lepton tensor [8], while the hadron tensor $N_{\lambda\lambda'}$, corresponding to breakup into three fragments with momenta $\hbar\mathbf{k}_1, \hbar\mathbf{k}_2$, and $\hbar\mathbf{k}_c$ for the halo neutrons and core, has the form

$$N_{\lambda\lambda'} = \frac{(2\pi)^6}{\hbar c} \overline{\sum} N_\lambda N^*_{\lambda'} \delta^4(q + P_i - P_f) d\mathbf{k}_1 d\mathbf{k}_2 d\mathbf{k}_c, \tag{2}$$

where $N_\lambda = \varepsilon^\mu_\lambda \langle \Psi_f, P_f | J_\mu(0) | \Psi_i, P_i \rangle$ denotes the nuclear matrix element of the electromagnetic current $J_\mu(0)$ between the initial and final nuclear states with total four-momenta $\hbar P_i$ and $\hbar P_f$, respectively. $\epsilon^\mu_\lambda$ are polarization vectors of the virtual photon with photon helicities $\lambda$. In the hadron tensor $N_{\lambda\lambda'}$ [Eq. (2)] the sum with the overbar includes averaging over initial target spin projections and summation over final ones for all fragments.

It is convenient to choose the coordinate system such that the $\hat{\mathbf{z}}$ axis is parallel to the transferred momentum $\hat{\mathbf{z}} \parallel \mathbf{q}$ and where the vector $\mathbf{k} = \mathbf{k}_i + \mathbf{k}_f$ lies entirely in the scattering $(\hat{\mathbf{x}}, \hat{\mathbf{z}})$-plane. The Jacobi momenta, $\hbar\mathbf{k}_x, \hbar\mathbf{k}_y$, and $\hbar\mathbf{P}_f$, used to characterize the motion of the fragments in the final nuclear state, are defined by the relations

$$\begin{aligned} \mathbf{k}_x &= \frac{\mu_x}{m_n}(\mathbf{k}_1 - \mathbf{k}_2), \mu_x = \frac{m_n}{2}, \\ \mathbf{k}_y &= \frac{\mu_y}{m_n}\left(\frac{\mathbf{k}_c}{A_c} - \frac{\mathbf{k}_1 + \mathbf{k}_2}{2}\right), \mu_y = \frac{2A_c}{A} m_n, \\ \mathbf{P}_f &= \mathbf{k}_1 + \mathbf{k}_2 + \mathbf{k}_c, \end{aligned} \tag{3}$$

where $\mu_{x,y}$ are reduced masses, $m_n$ is the nucleon mass, and $A$ and $A_c = A - 2$ are the number of nucleons in the nucleus and core, respectively. Phase space volume transforms as $d\mathbf{k}_1 d\mathbf{k}_2 d\mathbf{k}_c = d\mathbf{k}_x d\mathbf{k}_y d\mathbf{P}_f$. Vectors $\mathbf{q} \parallel \hat{\mathbf{z}}$ and $\mathbf{k}_y$ define the core ejectile plane, which relative to the scattering plane is tilted by the angle $\varphi$. If we choose a neutron as ejectile, a corresponding Jacobian coordinate system [9] should be used.

At this point we need to define more precisely our assumptions on nuclear structure. Our interest lies in studies of characteristic features of halo nuclei. Halo peculiarities are especially sensitive to the processes leading to the low-energy continuum excitations at small momentum transfers. Then the nonrelativistic Schrödinger equation is used for nuclear wave function calculations, and a nonrelativistic treatment of the current operator is applied. In addition, at small momentum transfers, which we are interested in here, the contributions from convection and magnetization currents can be neglected in comparison with the Coulomb interaction. This means that the contribution from the charge term $N_{00}$ in Eq. (1) dominates in inelastic scattering at such kinematical conditions, and only it is treated explicitly and kept in cross-section calculations below. The respective lepton tensor is $l_{00} = Q^2/|\mathbf{q}|^2$, where the square of the virtual photon wave vector $Q^2 = \mathbf{q}^2 - \omega^2/c^2$ appears. Then it can be shown [8] that the longitudinal part of nuclear current is given by

$$N_0 = \frac{\hbar W}{\mathcal{M}_i c} \frac{Q}{|\mathbf{q}|} \frac{1}{(2\pi)^3} \rho^{\rm ch}_{fi}(\mathbf{q}), \tag{4}$$

where $\hbar c W$ is the invariant mass of the final nuclear system and the calculation of the charge transition density $\rho^{\rm ch}_{fi}(\mathbf{q})$ is performed with wave functions in the nuclear c.m. frame [10]:

$$\begin{aligned} \rho^{\rm ch}_{fi}(q) = \int d\mathbf{r}'_1 \ldots d\mathbf{r}'_A \delta\left(\frac{1}{A}\sum_{j=1,A} \mathbf{r}'_j\right) \psi^{(-)*}_f(\mathbf{r}'_1, \ldots, \mathbf{r}'_A) \\ \times \sum_{j=1,Z} e^{i(\mathbf{q}\cdot\mathbf{r}'_j)} \psi_i(\mathbf{r}'_1, \ldots, \mathbf{r}'_A), \end{aligned} \tag{5}$$

where $Z$ is the number of protons and $\psi^{(-)}_f(\mathbf{r}'_1, \ldots, \mathbf{r}'_A)$ corresponds to a continuum state with ingoing wave boundary conditions. The nuclear wave functions $\psi_{i,f}$ depend on internal coordinates $\mathbf{r}'_j$ defined in the nuclear c.m. frame ($\sum_{j=1,A} \mathbf{r}'_j = 0$).

### B. Electron scattering within a three-body model of a Borromean halo nucleus

Here we specialize the general formalism presented above to the case of two-neutron Borromean halo nuclei. The basic dynamics can be characterized as a coexistence of two subsystems: one that consists of core nucleons and the other of halo neutrons moving relative to the core center of mass. With good accuracy the wave functions $\psi_{i,f}$ can be written as a product of two functions

$$\psi_{i,f}(\mathbf{r}'_1, \ldots, \mathbf{r}'_A) = \varphi_c(\boldsymbol{\xi}_1, \ldots, \boldsymbol{\xi}_{A_c}) \psi_{i,f}(\mathbf{x}, \mathbf{y}). \tag{6}$$

The function $\varphi_c(\boldsymbol{\xi}_1, \ldots, \boldsymbol{\xi}_{A_c})$ describes the internal structure of the core, while functions $\psi_{i,f}(\mathbf{x}, \mathbf{y})$ describe the relative motion of halo neutrons around the core c.m. In Eq. (6) the coordinate $\boldsymbol{\xi}_j$ denotes the position of a core nucleon relative the core c.m., $\mathbf{x}$ is the relative distance between halo neutrons, and $\mathbf{y}$ is the distance between the core and the center of mass of the two halo neutrons. Figure 1 shows the corresponding

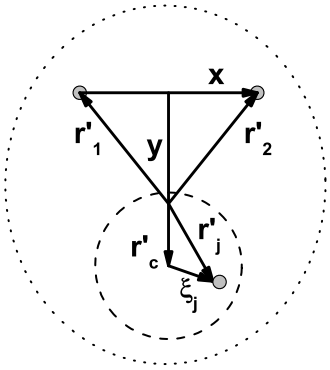


FIG. 1. Spatial coordinates in the nuclear c.m. frame.

coordinate system. The three-body continuum energy $E_\kappa$ above the three-body threshold is a sum of kinetic energies of relative motion of fragments, $E_\kappa = \varepsilon_x + \varepsilon_y = \hbar^2\mathbf{k}_x^2/2\mu_x + \hbar^2\mathbf{k}_y^2/2\mu_y$. Neglect of explicit considerations for internal core degrees of freedom is the main approximation in Eq. (6). These effects are treated approximately through the effective nucleon-core interaction. Such factorization is a starting point for application of three-body models to description of halo structure [9,11–18]. Few-body models avoid the complicated and still partly open questions concerning the development of nuclear clustering and instead calculate halo wave functions $\psi_{i,f}(\mathbf{x},\mathbf{y})$ directly. Within such models, extended for an approximate treatment of the Pauli principle, it is possible to give a consistent description of the main properties of both the ground state and the low-energy continuum wave functions of halo nuclei.

Applying factorization (6) and the coordinate transformation

$$d\mathbf{r}'_1 \dots d\mathbf{r}'_A \delta\left(\frac{1}{A}\sum_{j=1,A}\mathbf{r}'_j\right) = d\mathbf{x}\,d\mathbf{y}\delta \times \left(\frac{1}{A_c}\sum_{j=1,A_c}\boldsymbol{\xi}_j\right) d\boldsymbol{\xi}_1 \dots d\boldsymbol{\xi}_{A_c},$$

the charge transition density (5) can be written in product form as

$$\rho^{\rm ch}_{fi}(\mathbf{q}) = \rho^{\rm cm}_{fi}(\mathbf{q})\rho^{\rm ch}_c(\mathbf{q}) \tag{7}$$

where $\rho^{\rm ch}_c(\mathbf{q})$ is the core charge density and where $\rho^{\rm cm}_{fi}(\mathbf{q})$ describes the core c.m. motion,

$$\rho^{\rm cm}_{fi}(\mathbf{q}) = \int d\mathbf{x}\,d\mathbf{y}\ \psi^{(-)*}_f(\mathbf{x},\mathbf{y})e^{\imath\beta(\mathbf{q}\cdot\mathbf{y})}\psi_i(\mathbf{x},\mathbf{y})$$

$$\rho^{\rm ch}_c(\mathbf{q}) = \int d\boldsymbol{\xi}_1 \dots d\boldsymbol{\xi}_{A_c}\delta\left(\frac{1}{A_c}\sum_{j=1,A_c}\boldsymbol{\xi}_j\right) \times \sum_{j=1,Z} e^{\imath(\mathbf{q}\cdot\boldsymbol{\xi}_j)}|\varphi_c(\boldsymbol{\xi}_1,\dots,\boldsymbol{\xi}_{A_c})|^2, \tag{8}$$

where $\beta = 2/A$. Relative momenta of fragments and neutron spin projections on a quantization axis (we assume the core spin to be zero) are used to characterize uniquely the final continuum state $\psi^{(-)*}_f(\mathbf{x},\mathbf{y}) \equiv \psi^{(-)*}_{m_1,m_2}(\mathrm{k}_x,\mathrm{k}_y;\mathrm{x},\mathrm{y})$, while the initial nuclear total angular momentum $J_i$ and its projection $M_i$ are sufficient for the ground state identification, $\psi_i(\mathbf{x},\mathbf{y}) \equiv \psi_{J_iM_i}(\mathbf{x},\mathbf{y})$. For finding the bound and continuum states in the three-body structure model we use the method of hyperspherical harmonics [9]. In this method, the $^6$He continuum wave function has the decomposition

$$\psi^{(-)*}_{m_1,m_2}(\mathbf{k}_x,\mathbf{k}_y;\mathbf{x},\mathbf{y}) = \sum_{\gamma J_f M_f M_{L_f} M_{S_f}} \imath^{-K_f} \times \left(\frac{1}{2}m_1\frac{1}{2}m_2|S_fM_{S_f}\right) \times \left(L_fM_{L_f}S_fM_{S_f}|J_fM_f\right) \times [Y_{l_x}(\hat{\mathbf{k}}_x)\otimes Y_{l_y}(\hat{\mathbf{k}}_y)]_{L_fM_{L_f}} \times \psi^{l_x,l_y}_{K_f}(\theta_\kappa)\psi^*_{\gamma,J_fM_f}(\kappa,\mathbf{x},\mathbf{y}), \tag{9}$$

where $\gamma = \{l_x, l_y, L_f, S_f, K_f\}$ is an abbreviation for a set of quantum numbers, which characterizes the relative motion of the three fragments in $^6$He. $\psi^{l_x,l_y}_{K_f}(\theta_\kappa)$ is the hyperangular part of the hyperharmonic,

$$\psi^{l_x,l_y}_{K_f}(\theta_\kappa) = N^{l_xl_y}_{K_f}(\sin\theta_\kappa)^{l_x}(\cos\theta_\kappa)^{l_y} \times P^{l_x+1/2,l_y+1/2}_{(K_f-l_x-l_y)/2}(\cos 2\theta_\kappa), \tag{10}$$

where $P^{\alpha,\beta}_n$ are Jacobi polynomials and $N^{l_xl_y}_{K_f}$ is a normalization factor. The hyperangle $\theta_\kappa$ is defined as $\cos^2\theta_\kappa = \varepsilon_y/E_\kappa$. The continuum wave function $\psi_{\gamma,J_fM_f}(\kappa,\mathbf{x},\mathbf{y})$ depends on the Jacobian space coordinates $(\mathbf{x},\mathbf{y})$ shown in Fig. 1, the quantum numbers $\gamma$, the total angular momentum $J_f$ and its projection $M_f$, and the continuum energy $E_\kappa$, expressed by the hypermomentum $\kappa = \sqrt{2m_nE_\kappa/\hbar^2}$

$$\psi_{\gamma,J_fM_f}(\kappa,\mathbf{x},\mathbf{y}) = \frac{1}{(\kappa\rho)^{5/2}}\sum_{\gamma'}\chi^{J_f}_{\gamma,\gamma'}(\kappa,\rho) \times\psi^{l'_x,l'_y}_{K'_f}(\theta_\rho)[Y_{l'_x}(\hat{\mathbf{x}})\otimes Y_{l'_y}(\hat{\mathbf{y}})]_{L'M_{L'}} \times(L'M_{L'}S'M_{S'}|J_fM_f)|\chi_{S'M_{S'}}\rangle, \tag{11}$$

$$\tan\theta_\rho = \frac{\sqrt{\mu_x}|\mathbf{x}|}{\sqrt{\mu_y}|\mathbf{y}|},$$

$$\rho = \sqrt{\frac{\mu_x|\mathbf{x}|^2+\mu_y|\mathbf{y}|^2}{m_n}},$$

where $|\chi_{S'M_{S'}}\rangle$ is a coupled spin function for the two halo neutrons. The hyperradial wave function $\chi^{J_f}_{\gamma,\gamma'}(\kappa,\rho)$ is a solution of a set of the coupled $K$-harmonic equations. The ground state wave function $\psi_{J_iM_i}(\mathbf{x},\mathbf{y})$ has a similar decomposition to $\psi_{\gamma,J_fM_f}(\kappa,\mathbf{x},\mathbf{y})$[Eq. (11)] but now with $\kappa = \sqrt{2m_n|E_B|/\hbar^2}$, with separation energy $|E_B|$. The necessary details on how to solve a system of $K$-harmonic equations and on how to choose the nucleon-nucleon and nucleon-core potentials of the three-body bound and continuum wave functions can be found in Ref. [9]. By using the decompositions given above, a core transition density, which is a reduced matrix element between initial and final nuclear states and describes the system

response to a zero-range perturbation and also describes its Fourier image, can be calculated [15,18]:

$$\rho^{l0l}_{\gamma J_f,J_i}(\kappa,r) = \langle \psi_{\gamma,J_f}(\kappa) \| \frac{\delta(r-r'_c)}{r_c^2} Y_l(\hat{y}) \| \psi_{J_i} \rangle,$$
$$\rho^{l0l}_{\gamma J_f,J_i}(\kappa,q) = \int_0^\infty dr\, r^2\, j_l(qr) \rho^{l0l}_{\gamma J_f,J_i}(\kappa,r), \qquad (12)$$

where $\mathbf{r}'_c = \beta \mathbf{y}$ is the core c.m. radius. The quantum numbers $l$, $s$, and $j$ in the transition density $\rho^{lsj}_{\gamma J_f,J_i}$ correspond to the orbital, spin, and total angular-momentum transfers, respectively. Since the $\alpha$-particle core has zero spin and the core is not destroyed in the reaction, only excitations of natural parity states ($l = j$) in $^6$He with the spin transfer $s = 0$ are possible. Transition densities of halo neutrons do not appear explicitly in the expressions below because we take into account only the Coulomb interaction of electrons with the charge of the core constituent.

Choosing the energy $E_\kappa$ as an independent variable instead of the electron energy $\varepsilon_f$, the hadron tensor $N_{00}$ in (2) can be integrated,

$$\int d\varepsilon_f N_{00} = d\hat{\mathbf{k}}_x\, d\hat{\mathbf{k}}_y\, d\varepsilon_y\, dE_\kappa\, f_R 2 \left(\frac{\mu_x\mu_y}{\hbar^4}\right)^{3/2} \times \sqrt{\varepsilon_y(E_\kappa-\varepsilon_y)}\, \frac{Q^2}{|\mathbf{q}|^2} \frac{(\hbar W)^2}{(\mathcal{M}_i c)^2} W_{00}.$$

Here the recoil factor $f_R$ is given by

$$f_R = \left[1 + \frac{\varepsilon_f}{\mathcal{M}_i c^2}\left(1 - \frac{|\mathbf{k}_i|\cos\theta}{|\mathbf{k}_f|}\right)\right]^{-1}, \qquad (13)$$

and the final electron energy $\varepsilon_f$ is defined by energy conservation. The factor $\sqrt{\varepsilon_y(E_\kappa-\varepsilon_y)}$ is the phase space accessible to decay into fragments. The nuclear structure function $W_{00}$ is given by

$$W_{00} = \frac{[\rho_c^{\rm ch}(\mathbf{q})]^2}{\hat{J}_i^2} \sum_{m_1 m_2 M_i} |\langle \psi^{(-)}_{m_1 m_2}(\mathbf{k}_x,\mathbf{k}_y)| e^{\imath\beta(\mathbf{q}\cdot\mathbf{y})} |\psi_{J_i M_i}\rangle|^2, \qquad (14)$$

where $\hat{J} = \sqrt{2J+1}$. Using decomposition (9) and definition (12) and performing summations over spin projections, the structure function can be written as

$$\begin{aligned} W_{00} = {} & \frac{1}{\hat{J}_i^2} \sum_\delta \frac{\sqrt{4\pi}}{\hat{L}} \left( \left[ Y_{L_x}(\hat{\mathbf{k}}_x) \otimes Y_{L_y}(\hat{\mathbf{k}}_y) \right]_L \cdot Y_L(\hat{\mathbf{q}}) \right) \\ & \times (-1)^{J_i+S_f+L_f+J_f+J'_f+l'_x+l'_y} \imath^{l-l'+K'_f-K_f} \\ & \times \psi^{l_x,l_y}_{K_f}(\theta_\kappa) \psi^{l'_x,l'_y}_{K'_f}(\theta_\kappa) \hat{l}\hat{l}_x\hat{l}_y\hat{L}_f\hat{J}_f\hat{l}'\hat{l}'_x\hat{l}'_y\hat{L}'_f\hat{J}'_f \\ & \times (l_x 0 l'_x 0|L_x 0)(l_y 0 l'_y 0|L_y 0)(l0l'0|L0) \\ & \times \begin{Bmatrix} L_f & L'_f & L \\ J'_f & J_f & S_f \end{Bmatrix} \begin{Bmatrix} J_f & J'_f & L \\ l' & l & J_i \end{Bmatrix} \begin{Bmatrix} l'_y & l'_x & L'_f \\ l_y & l_x & L_f \\ L_y & L_x & L \end{Bmatrix} \\ & \times \rho^{l0l}_{\gamma J_f,J_i}(\kappa,q) \rho^{l'0l'*}_{\gamma' J'_f,J_i}(\kappa,q) (\rho_c^{\rm ch}[\mathbf{q}])^2. \end{aligned} \qquad (15)$$

Here the index $\delta$ includes all quantum numbers and intermediate summation indices. Since we averaged over fragment spin projections, the interference between motions with different values of the total spin $S_f$ of the two neutrons is lost, and excitations with different $S_f$ give independent contributions to cross sections. The function $W_{00}$ contains all information about the nuclear structure, energy, and angular correlations of the fragments. The exclusive cross section of electron scattering, leading to the low-energy excitations of $^6$He, is now equal to

$$\frac{d^8\sigma}{d\hat{\mathbf{k}}_f d\hat{\mathbf{k}}_x d\hat{\mathbf{k}}_y dE_\kappa d\varepsilon_y} = f_R \sigma_M 2 \left(\frac{\mu_x\mu_y}{\hbar^4}\right)^{3/2} \sqrt{\varepsilon_y(E_\kappa-\varepsilon_y)} \times \frac{Q^4}{|\mathbf{q}|^4} \frac{(\hbar W)^2}{(\mathcal{M}_i c)^2} W_{00}. \qquad (16)$$

This cross section contains the most complete information that can be extracted from a reaction that is a breakup into three fragments with unpolarized electrons at small transferred momenta. Cross section (16) depends, however, on too many variables to offer a meaningful analysis of the important correlations. It is more instructive to integrate out most of the independent variables and analyze various inclusive cross sections, and thus clarify the underlying dynamics. So, many different energy and angular correlations can be singled out that contain valuable information about the nuclear structure of halo nuclei.

A variety of the different motion modes connected with relative momenta $\mathbf{k}_x$ and $\mathbf{k}_y$ are characterized by some subset of quantum numbers and coexist in the final system. The modes interfere with one another and give a coherent contribution to the exclusive cross sections (16). Integration over momentum destroys the interference, and the corresponding motion modes add independent contributions to cross sections. Therefore different cross sections are sensitive to different correlations, and simultaneous descriptions of all of them within the framework of one model give a thorough test of the underlying dynamics and model assumptions of nuclear structure and reaction mechanisms. Detecting electrons, we know the momentum $\mathbf{q}$ that is transferred to the nucleus and the energy $E_\kappa$. If, in addition, the core momentum $\mathbf{k}_c$ is measured, we also know the relative momentum $\mathbf{k}_y$ and the absolute value $|\mathbf{k}_x|$. The corresponding cross section is obtained by integration over the unobserved direction $\hat{\mathbf{k}}_x$:

$$\begin{aligned} \int d\hat{\mathbf{k}}_x W_{00} = {} & \frac{1}{\hat{J}_i^2} \sum_{\delta'} (-1)^{L+J_i+S_f+J_f+J'_f+l_x} \\ & \times \imath^{l-l'+K'_f-K_f} \psi^{l_x,l_y}_{K_f}(\theta_\kappa) \psi^{l_x,l'_y}_{K'_f}(\theta_\kappa) P_L(\hat{\mathbf{q}}\cdot\hat{\mathbf{k}}_y) \\ & \times \hat{l}\hat{l}_y\hat{L}_f\hat{J}_f\hat{l}'\hat{l}'_y\hat{L}'_f\hat{J}'_f (l_y 0 l'_y 0|L0)(l0l'0|L0) \\ & \times \begin{Bmatrix} L_f & L'_f & L \\ J'_f & J_f & S_f \end{Bmatrix} \begin{Bmatrix} J_f & J'_f & L \\ l' & l & J_i \end{Bmatrix} \begin{Bmatrix} l_y & l'_y & L \\ L'_f & L_f & l_x \end{Bmatrix} \\ & \times \rho^{l0l}_{\gamma J_f,J_i}(\kappa,q) \rho^{l'0l'*}_{\gamma' J'_f,J_i}(\kappa,q) \left[\rho_c^{\rm ch}(\mathbf{q})\right]^2, \end{aligned} \qquad (17)$$

where $\delta' = (L, S_f, l_x, l, J_f, L_f, l_y, K_f, l', J'_f, L'_f, l'_y, K'_f)$. This integration destroys the angular correlation of the $\mathbf{k}_x$ motion, so modes with different values of the angular orbital moment $l_x$ give independent contributions to nuclear excitations. Distribution (17) depends on the angle between the transferred momentum $\hat{\mathbf{q}}$ and the direction $\hat{\mathbf{k}}_y$ of the core

fragment decay. The integration over $\hat{\mathbf{k}}_y$ destroys all angular correlations in the fragment motion

$$\int d\hat{\mathbf{k}}_x d\hat{\mathbf{k}}_y W_{00} = \frac{4\pi}{\hat{J}_i^2} \sum_{\delta''} \imath^{K'_f - K_f} \psi^{l_x,l_y}_{K_f}(\theta_\kappa)\psi^{l_x,l_y}_{K'_f}(\theta_\kappa)\rho^{l0l}_{\gamma J_f,J_i} \times (\kappa,q)\rho^{l0l*}_{\gamma' J_f,J_i}(\kappa,q)\left[\rho_c^{\rm ch}(\mathbf{q})\right]^2,$$

where $\delta'' = (l, J_f, S_f, L_f, l_x, l_y, K_f, K'_f)$, but still keeps the information about energy correlations, i.e., how the excitation energy is distributed between the fragments. Using the orthonormality condition of hyperharmonics,

$$\int_0^{E_\kappa} d\varepsilon_y \sqrt{\varepsilon_y(E_\kappa - \varepsilon_y)}\, \psi^{l_x,l_y}_{K_f}(\theta_\kappa)\psi^{l_x,l_y}_{K'_f}(\theta_\kappa) = 2E_\kappa^2 \delta_{K_f K'_f},$$

the integration over all possible fragment energies $\varepsilon_y$ at fixed excitation energy $E_\kappa$ can be performed. Then the inclusive cross section for electron inelastic scattering can be obtained

$$\frac{d^3\sigma}{d\hat{\mathbf{k}}_f dE_\kappa} = f_R \sigma_M \left(\frac{\mu_x\mu_y}{\hbar^4}\right)^{3/2} 4E_\kappa^2 \frac{Q^4}{|\mathbf{q}|^4}\frac{(\hbar W)^2}{(\mathcal{M}_i c)^2} \times \frac{4\pi}{\hat{J}_i^2}\sum_{lJ_f\gamma} \left|\rho^{l0l}_{\gamma J_f,J_i}(\kappa,q)\right|^2\left[\rho_c^{\rm ch}(\mathbf{q})\right]^2. \quad (18)$$

For the low excitation energy $E^*$ (= $E_\kappa$ + $|E_B|$) considered here, the factor $\hbar W/\mathcal{M}_i c = 1 + E^*/\mathcal{M}_i c^2 \simeq 1$.

## III. RESULTS

### A. Elastic scattering

The elastic electron scattering cross section on a Borromean halo nucleus can be written in the following form

$$\frac{d\sigma}{d\hat{\mathbf{k}}_f} = f'_R \sigma_M \frac{Q^4}{\mathbf{q}^4} Z^2 |F_{\rm ch}(q)|^2,$$

$$|F_{\rm ch}(q)|^2 = \frac{1}{Z^2}\frac{4\pi}{\hat{J}_i^2}\sum_l \left|\rho^{l0l}_{J_i}(q)\right|^2\left[\rho_c^{\rm ch}(\mathbf{q})\right]^2, \quad (19)$$

$$f'_R = \left(1 + \frac{2\varepsilon_i}{\mathcal{M}_i c^2}\ \sin^2\frac{\theta}{2}\right)^{-1},$$

where $\rho^{l0l}_{J_i}(q)$ is a density describing the core c.m. motion in the ground state, defined by Eq. (12) but with the ground state wave function $\psi_{J_i}$ used on the left-hand side of the matrix element instead of $\psi_{\gamma,J_f}(\kappa)$. Since the spin of the $^6$He ground state is equal to zero, only the value zero of the transferred orbital momentum $l$ is allowed in Eqs. (19). From Eqs. (19) follows that the charge form factor $F_{\rm ch}(q)$ of the halo nucleus within the cluster model is proportional to the product of the core charge form factor $\rho_c^{\rm ch}(\mathbf{q})$ and the density $\rho^{l0l}_{J_i}(q)$ for motion of the core c.m. in momentum space. Note that in article [1] one could get the impression that the charge form factor $F_{\rm ch}(q)$ is identical to the core charge form factor $\rho_c^{\rm ch}(\mathbf{q})$, which would be wrong.

In our recent article [19] we presented calculations of the $^6$He charge form factor within the three-body model and made comparisons with the experimentally known $^4$He form factor and also to the small momentum behavior defined by the r.m.s. charge radius of $^6$He, $F_{\rm ch}(q) \simeq 1 - \langle r_{\rm ch}^2\rangle \mathbf{q}^2/6$. The charge

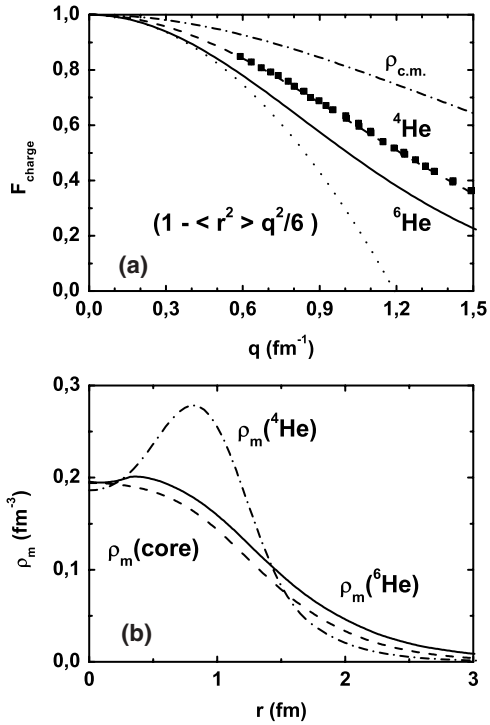


FIG. 2. (a) Charge form factors and (b) matter densities. The curves are described in the text.

radius, $\sqrt{\langle r_{\rm ch}^2\rangle} = 2.054 \pm 0.014$ fm, was measured recently by the method of laser spectroscopy in [21]. Figure 2 (a) shows the various charge form factors. The phenomenological Woods-Saxon fit to the charge form factor of $^4$He [20], extracted from the experimental data (black squares) on electron scattering is shown by the dashed curve. The calculated density $\sqrt{4\pi}\rho^{l0l}_{J_i}(q)$ for the c.m. motion of the $^4$He core inside the $^6$He nucleus is given by the dashed-dotted curve. The corresponding product charge form factor of $^6$He is presented by the solid curve, while the small momentum approximation using the experimental value of the charge radius is shown by a dotted curve. The charge radius defines the behavior of the charge form factor for momentum $q \leqslant 0.5$ fm$^{-1}$. At larger momenta the finer details of the charge density become important. Comparison of measurements (they will be possible at the future installations at RIKEN and GSI) with theoretical calculations may probe our halo picture. Within the cluster model the charge form factor is completely defined by the product of internal core form factor and that for core c.m. motion. Thus deviations of experimental data from calculations may indicate a changing of core properties inside the nucleus (core polarization) due to interactions with halo neutrons. The position of the $^6$He charge form factor minimum must, according to the cluster model, coincide with the position of the minimum for $^4$He. Checking this prediction will test the reliability of cluster models at high momentum, but this will be a difficult experimental task that requires measurements for transferred momenta larger then 3 fm$^{-1}$.

The behavior of different matter densities in coordinate space is shown in Fig. 2(b). Here, the matter density of $^4$He (double charge density of pointlike protons), extracted from

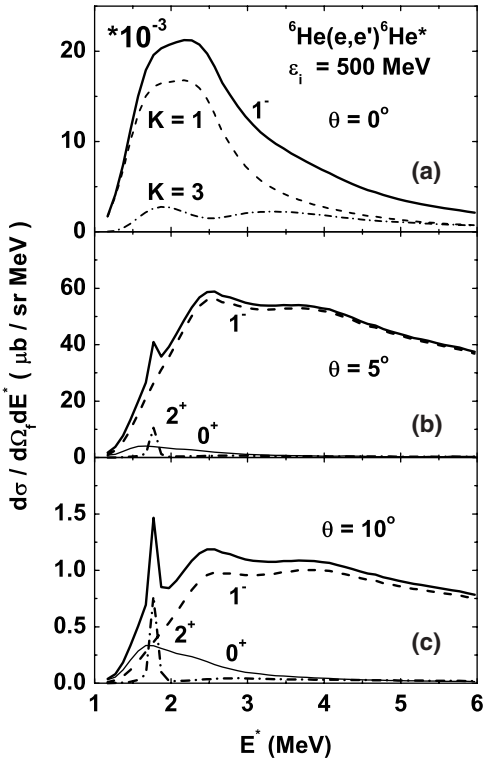


FIG. 3. Inclusive inelastic electron scattering on $^6$He for $\varepsilon_i =$ 500 MeV and various scattering angles. (a) The solid curve is the total (dipole) cross section. The dashed and dotted-dashed curves are contributions to the dipole excitation from modes with orbital momenta $l_x = 0, l_y = 1$, spin $S_f = 0$, hypermoments $K_f = 1, 3$, respectively. (b), (c) The solid, dashed, dotted-dashed, and thin solid curves are the total, dipole, quadrupole, and monopole cross sections, respectively.

the experimentally known charge density [20], is given by the dashed-dotted curve. The corresponding core density obtained by folding with the motion of the core c.m. is shown by the dashed curve. The matter density of $^6$He, which in addition to the core includes contribution from the halo neutrons, is presented by the solid curve. This figure demonstrates the important role of the core c.m. motion in creating a smoother density behavior.

### B. Inelastic scattering

As an example of inclusive electron scattering, we consider an electron collision with $^6$He at an initial energy $\varepsilon_i =$ 500 MeV, which will become available at GSI. Figure 3 shows the calculated spectra of low-energy excitations for a few scattering angles $\theta$ corresponding to transferred momenta $|\mathbf{q}| <$ 80 (MeV/$c$). The absolute cross sections depend strongly on the momentum transfer $|\mathbf{q}|$ and decrease rapidly with increasing electron scattering angle $\theta$. The multipole composition of excitation spectra depends on properties of the Coulomb interaction and the nuclear structure. In the multipole decomposition of the Coulomb interaction the monopole term decreases most slowly with the distance between the electron and the nuclear center of mass, and then follow terms with higher angular momenta, dipole, quadrupole, and so on. At small momentum transfer a reaction amplitude gets its main contribution from large distances, where, however, the monopole excitations are strongly suppressed by the orthogonality of the ground and continuum halo states. As a result the dipole excitations dominate at the low excitation energies for small $|\mathbf{q}|$ [Fig. 3(a)]. For dipole excitations there are two main decay channels having the highest matching with the ground state. The first is the $p_{3/2}$ ground state of $^5$He, for which the internal part of the wave function is amplified in the compact region by strongly overlapping with the ground state of $^6$He. It is also kinematically favorable that the second neutron is in a $s_{1/2}$ state with zero centrifugal barrier. This channel has the simplest representation in a Jacobi system rotated relative to the one we use here. The second channel, due to dipole transition from the $^6$He ground state (with a 85% component $l_x = 0, l_y = 0$), is the singlet neutron-neutron $s$-wave virtual state ($l_x = 0$) with relative orbital angular momentum $l_y = 1$ between the two halo neutrons and the core. Therefore components with $l_x = 0, l_y = 1$ and hypermoments $K_f \geqslant 1$ will dominate the dipole transition. These modes, giving the main contributions to excitations with hypermoments $K_f = 1, 3$, are shown by the dashed and dotted-dashed curves in Fig. 3(a).

In Figs. 3(b) and 3(c) the solid, dashed, dotted-dashed, and thin solid curves are the total, dipole, quadrupole, and monopole excitations of $^6$He, respectively. With increasing momentum transfer the well-known three-body $2^+$ resonance at $E^* = 1.8$ MeV appears [Fig. 3(b)] and soon becomes a pronounced feature [Fig. 3(c)] in the low-energy spectrum. If part of the FSI is neglected in the calculations, two effects happen.

Firstly the orthogonality of the ground and continuum states is lost, and the monopole excitations dominate the spectrum near the breakup threshold, a physically wrong result for electromagnetic processes. Secondly the $2^+$ resonance disappears from the spectrum. Thus the final state interactions are an essential part of the reaction dynamics of the low-energy excitations. The concentration of the dipole transition strength near threshold does not mean that dipole excitations have a collective nature and represent a resonance. As seen from Figs. 3(a)–3(c), the energy position and the shape of the dipole excitations show a strong dependence on transferred momentum, while for a genuine three-body resonance, like the $2^+$ at $E^* = 1.8$ MeV, the peak position is fixed. To further clarify the true nature of the observed $1^-$ peak, more complicated energy correlations of the fragments must be studied.

### C. Coincidence cross sections

We now turn to breakup cross sections where the $\alpha$ particle is detected in coincidence with the scattered electron. Then the energy and angle of the $\alpha$ particle characterize the cross section in addition to electron degrees of freedom. Note that in the nuclear rest frame ($\mathbf{P}_f = 0$) $\hbar\mathbf{k}_y$ is equal to the $\alpha$-particle momentum. Since we consider processes with small momentum and energy transfers for which the Coulomb interaction dominates, the coincidence cross section does not depend on the angle $\varphi$, the orientation of the ejectile plane relative to the scattering plane. As seen from Eq. (17),

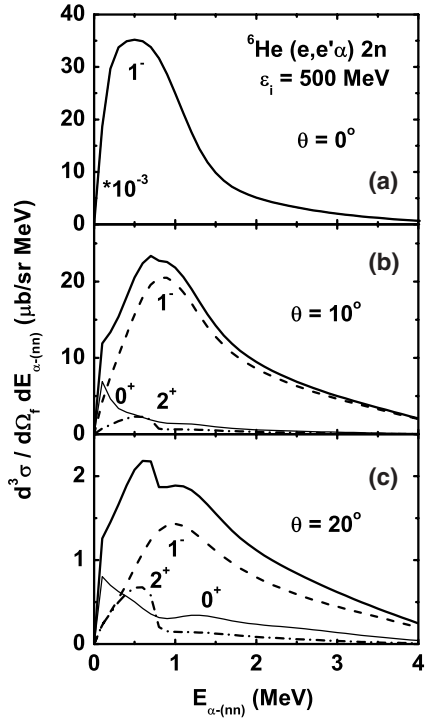


FIG. 4. Coincidence cross sections $d^3\sigma/d\Omega_f dE_\alpha$ for electron scattering on $^6$He at $\varepsilon_i = 500$ MeV and various angles. The solid, dashed, dotted-dashed, and thin solid curves are the total, dipole, quadrupole, and monopole cross sections, respectively.

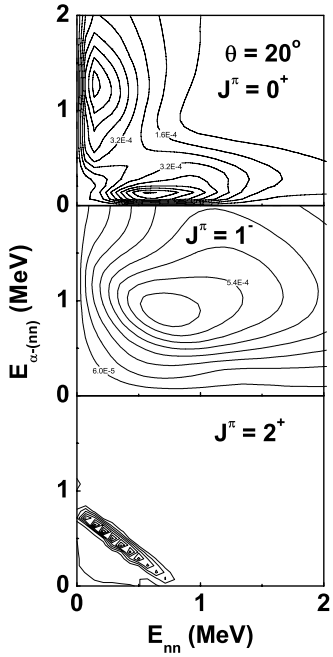


FIG. 5. Contour plots of electron cross sections for separate multipole excitations for scattering angle $\theta = 20^\circ$ as function of the relative energy between the two halo neutrons $E_{nn}$ and their energy relative the $\alpha$-particle $E_{\alpha-(nn)}$.

in addition to the electron variables, the reaction dynamics depends on the relative angle between the momenta $\hbar\mathbf{k}_y$ and $\hbar\mathbf{q}$ and the $\alpha$-particle energy ($=\varepsilon_y/3$ in the rest frame).

To further reduce the number of independent variables, we consider distributions over the relative energy $E_{\alpha-(nn)}$ ($=\varepsilon_y$) between the $\alpha$ particle and the c.m. of the halo neutron pair, $d^3\sigma/d\Omega_f dE_{\alpha-(nn)}$, which is obtained by integrating the exclusive cross sections over the $\alpha$-particle direction $\hat{\mathbf{k}}_y$ and over the total nuclear excitation energy $E^*$ from the breakup threshold up to 6 MeV. Figure 4 shows these cross sections for a few electron scattering angles. The solid, dashed, dotted-dashed, and thin solid curves give the total, dipole, quadrupole, and monopole contributions, respectively. Dipole excitations dominate the spectra. The dipole shape changes with increasing transferred momentum $\mathbf{q}$, in particular, the position of the maximum is shifted to larger energies with increasing $\mathbf{q}$. Such changes are evidence that the dipole excitations are not a real resonance. The $\alpha$-particle contributions from monopole and quadrupole excitations become noticeable at larger transferred momenta. They have different shapes. The quadrupole is defined by breakup of the well-known $2^+$ resonance and has a very specific shape. The $\alpha$'s from monopole excitations have a significant part at small energies. To better demonstrate the decay properties of multipole excitations, Fig. 5 shows contour plots of cross sections for separate multipolarities as function of the relative energies $E_{nn}$ ($=\varepsilon_x$) and $E_{\alpha-(nn)}$. The decay patterns of the energy correlations are distinctly different for the different multipole excitations. For quadrupole excitation the decays are stretched along a straight line, which is a clear signal of resonance behavior (see Ref. [22] and relevant discussions there). Monopole correlations reveal two peaks: one, where the $\alpha$ particle is at rest and two neutrons carry all excitation energy, and the other where the two neutrons have low relative energy and the excitation energy is defined by the relative motion between the $\alpha$ and the neutron pair. This picture keeps an imprint of the cigar and dineutron configurations in the ground state structure of $^6$He [11].

Next we consider the angular correlations in coincidence cross sections. Again, to reduce the number of independent variables, we integrate Eq. (17) over relative energy $\varepsilon_y$ and calculate cross sections $d^5\sigma/d\Omega_f d\Omega_y dE^*$ as a function of the angle $\theta_{\alpha q}$ between the $\alpha$ particle and the transferred momentum $\mathbf{q}$. Before demonstration of general cases, it is instructive to look at coincidence cross sections for single multipole excitation. Taking into account that at low-energy excitations the motions with lowest possible orbital momenta dominate, for the dipole in $^6$He we can obtain from Eq. (17) the following expression:

$$\frac{d^5\sigma}{d\Omega_f d\Omega_y dE^*} = \frac{1}{4\pi}\frac{d^3\sigma}{d\Omega_f dE^*}\{1 + 2P_2(\hat{\mathbf{q}}\cdot\hat{\mathbf{k}}_y)S_1\}.$$

Here $S_1$ denotes the structure factor for dipole excitations and is equal to

$$S_1 = S(l_x = 0, l_y = 1) + \frac{1}{2}S(l_x = 1, l_y = 2) + \frac{1}{10}S(l_x = 2, l_y = 1) + \cdots, \qquad (20)$$
$$S(l_x, l_y) = \left|\rho^{101}_{\gamma J_f J_i}(\kappa, q)\right|^2 \Big/ \sum_{\gamma'}\left|\rho^{101}_{\gamma' J_f J_i}(\kappa, q)\right|^2.$$

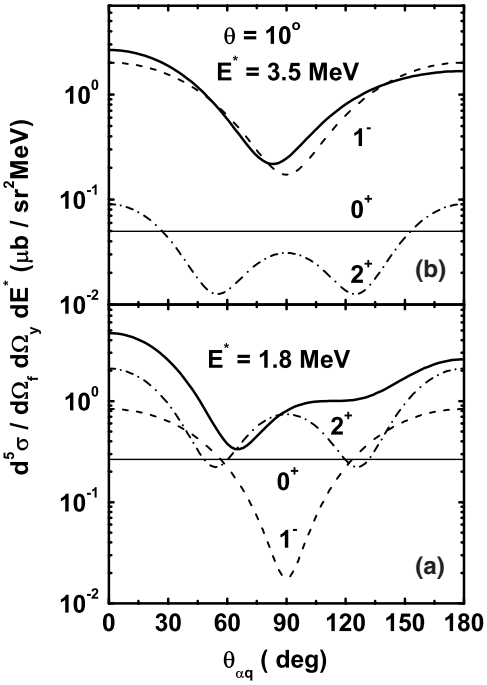


FIG. 6. Cross sections $d^5\sigma/d\Omega_f d\Omega_y dE^*$ for electrons with energy $\varepsilon_i = 500$ MeV and scattering angle $\theta = 10^\circ$ as function of the relative angle $\theta_{\alpha q}$ between the $\alpha$ particle and transferred momentum $\mathbf{q}$. Parts (a) and (b) correspond to 1.8 MeV and 3.5 MeV excitation energies in $^6$He, respectively. The solid, dashed, dotted-dashed and thin solid curves are the total, dipole, quadrupole, and monopole contributions.

The factor $S(l_x, l_y)$ gives the weight that the mode of motion described by the corresponding quantum numbers has in the total transition from the ground state to continuum at given excitation energy. Terms corresponding to larger orbital angular momenta and interference from excitations with fixed quantum numbers $(S_f, l_x)$ and different $l_y$ are not shown explicitly in Eq. (20). They are not large at excitations near breakup threshold. It is important to note that the angular dependence is defined by the presence of motion modes with $l_y > 0$. Components with $l_y = 0$ give contributions to the isotropic part of the cross sections defined by the Legendre polynomials $P_L$ with $L = 0$. Only via small possible interference terms with modes having nonzero values of $l_y$ is angular dependence induced in the cross sections. A corresponding analysis can be done for quadrupole excitations. It leads to analogous expressions but with a more complicated angular dependence that includes some combination of the Legendre polynomials of orders 2 and 4.

Figure 6 shows examples of the $\theta_{\alpha q}$ angular correlations for two different excitation energies in $^6$He: the $2^+$ resonance is largest in part (a) and the dipole excitation dominates in (b). The shapes of the distributions are different for different multipolarities, and symmetric relative 90°. The monopole has an isotropic distribution. The dipole has a pronounced minimum at 90° while the quadrupole has two minima near 60° and 120° and maximum at 90° with a height a few times less then at 0° or 180°. The total distribution includes contributions not only from separate multipole excitations

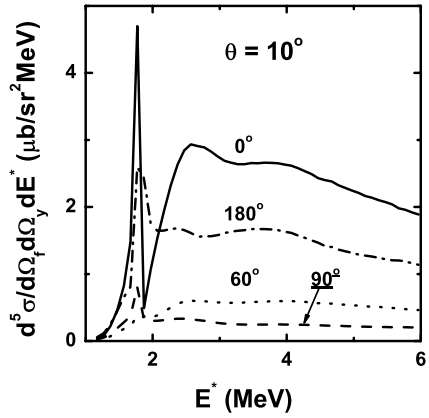


FIG. 7. Cross sections $d^5\sigma/d\Omega_f d\Omega_y dE^*$ for electrons with energy $\varepsilon_i = 500$ MeV and scattering angle $\theta = 10^\circ$ as function of nuclear excitation energy $E^*$. The solid, dotted, dashed, and dotted-dashed curves correspond to angles $\theta_{\alpha q}$ equal 0°, 60°, 90°, and 180°, respectively.

but also their interference. As a result, the total distribution is not symmetrical relative to 90° and can have a rather complicated shape as, for example, in Fig. 6(a), where dipole and quadrupole are excited with comparable strength. In cases when one multipole excitation dominates as, for example, in Fig. 6(b), the total distribution keeps a shape that is specific for the single multipole and only slightly distorted. Thus it can give a clear signal on the multipole nature of dominant nuclear excitations. Then the analysis given above can be applied. If, for example, dipole correlations with deep minimum will be observed that will exclude a large weight for motion with $l_y = 0$ in the energy region of the excitation spectrum which is under investigation.

Finally, Figure 7 shows coincidence spectra $d^5\sigma/d\Omega_f d\Omega_y dE^*$ for electron scattering angle $\theta = 10^\circ$ as function of the nuclear excitation energy $E^*$ for different angles $\theta_{\alpha q}$. In the energy region of the $2^+$ resonance the multipole interference strongly influences the shape of the spectrum. For angle $\theta_{\alpha q} = 0^\circ$ (solid curve) this results in a separation of $2^+$ and dipole, while at 180° (dotted-dashed curve) there is no gap between. At 60° (dotted curve) the $2^+$ is much more strongly suppressed than other multipoles, giving a smooth spectrum without a resonance peak.

## IV. CONCLUSION

We have developed a theory for description of electron scattering from two-neutron Borromean halo nuclei in which effects of final state interactions between fragments are fully taken into account. The theory is coined for processes with small transferred momenta leading to low-energy nuclear excitations, the region which is most sensitive to the specific features of halo structure. The participant-spectator model is not applicable to this region. The nuclear structure was described within a cluster three-body model. This model not only reproduces rather well the properties of the ground state but is the natural basis for calculation of continuum states

when the nucleus breaks into three fragments. The method of hyperspherical harmonics was used for solution of the three-body problem and for calculations of transition densities to the continuum.

The theory has been applied to make predictions for electron scattering from $^6$He, the Borromean nucleus which is the test-bench example for theoretical studies of two-neutron halo structure. Our calculations of inclusive inelastic scattering show that dipole excitations dominate in the spectrum at small transferred momenta. The position of the maximum and the shape of the dipole spectrum change with increasing transferred momenta. This differs from the behavior of the well-known $2^+$ true three-body resonance and gives additional evidence against a resonance nature for the soft dipole excitations.

Future measurements of electrons in coincidence with fragments promise to give valuable information about the halo structure. The pattern of energy and angular correlations are rather specific for different multipole excitations. Correlation measurements in general provide a unique tool for revealing the complex dynamics of nuclear excitations and pave the way to spectroscopy of the continuum, granted that rather small cross sections can be measured.

## ACKNOWLEDGMENTS

S. N. Ershov and B. V. Danilin are thankful to the University of Bergen for hospitality and acknowledge support from RFBR grants 02-02-16174 and 1885.2003.2. B. V. Danilin acknowledges support from grant INTAS 03-54-6545.

[1] E. Garrido and E. Moya de Guerra, Nucl. Phys. **A650**, 387 (1999).
[2] E. Garrido and E. Moya de Guerra, Phys. Lett. **B488**, 68 (2000).
[3] S. Ishikawa *et al*., Nuovo Cimento **A107**, 305 (1994).
[4] J. Golak, H. Witala, H. Kamada, D. Hüber, S. Ishikawa, and W. Glöckle, Phys. Rev. C **52**, 1216 (1995).
[5] J. D. Bjorken, S. D. Drell, *Relativistic Quantum Mechanics* (McGraw Hill, New York, 1964).
[6] T. D. de Forest and J. D. Walecka, Adv. Phys. **15**, 1 (1966).
[7] C. Ciofi degli Atti, Prog. Part. Nucl. Phys. **3**, 163 (1980).
[8] V. Dmitrasinovic and F. Gross, Phys. Rev. C **40**, 2479 (1989).
[9] B. V. Danilin, I. J. Thompson, M. V. Zhukov, and J. S. Vaagen, Nucl. Phys. **A632**, 383 (1998).
[10] J. L. Friar and M. Rosen, Ann. Phys. (NY) **87**, 289 (1974).
[11] M. V. Zhukov B. V. Danilin, D. V. Fedorov *et al*., Phys. Rep. **231**, 151 (1993).
[12] B. V. Danilin and M. V. Zhukov, Yad. Fiz. **56**, 67 (1993) [Phys. At. Nucl. **56**, 460 (1993)].
[13] D. V. Fedorov, A. S. Jensen, and K. Riisager, Phys. Rev. C **50**, 2372 (1994).
[14] B. V. Danilin, M. V. Zhukov, S. N. Ershov, F. A. Gareev, R. S. Kurmanov, J. S. Vaagen, and J. M. Bong Phys. Rev. C **43**, 2835 (1991).
[15] S. N. Ershov, T. Rogde, B. V. Danilin, J. S. Vaagen, I. J. Thompson, and F. A. Gareev, Phys. Rev. C **56**, 1483 (1997).
[16] S. N. Ershov, B. V. Danilin, T. Rogde, and J. S. Vaagen, Phys. Rev. Lett. **82**, 908 (1999).
[17] S. N. Ershov, B. V. Danilin, and J. S. Vaagen, Phys. Rev. C **62**, 041001(R) (2000).
[18] S. N. Ershov, B. V. Danilin, and J. S. Vaagen, Phys. Rev. C **64**, 064609 (2001).
[19] B. V. Danilin, S. N. Ershov, and J. S. Vaagen, Phys. Rev. C **71**, 057301 (2005).
[20] J. S. McCarthy, I. Sick, and R. R. Whitney, Phys. Rev. C **15**, 1396 (1977).
[21] L.-B. Wang *et al*., Phys. Rev. Lett. **93**, 142501 (2004).
[22] S. N. Ershov, B. V. Danilin, J. S. Vaagen, A. A. Korsheninnikov, and I. J. Thompson, Phys. Rev. C **70**, 054608 (2004).